Polym. Bull. (2017) 74:997–1010
DOI 10.1007/s00289-016-1759-3

ORIGINAL PAPER

# Synergetic association of grafted PLA and functionalized graphene on the properties of the designed nanocomposites

**Kahina Issaadi[1,2] · Isabelle Pillin[2] · Abderrahmane Habi[1] · Yves Grohens[2]**

Received: 10 June 2015 / Revised: 11 July 2016 / Accepted: 15 July 2016 /
Published online: 26 July 2016
© Springer-Verlag Berlin Heidelberg 2016

**Abstract** The synergetic association of poly(lactic acid) grafted with maleic anhydride (MA-*g*-PLA) containing 0.44 wt% of maleic anhydride and epoxy-functionalized graphene (GFe) on the properties of the designed nanocomposites was studied. Rheological, mechanical and barrier properties of PLA nanocomposites were studied using different content of epoxy-functionalized graphene and MA-*g*-PLA compatibilizer. The PLA/MA-*g*-PLA/GFe nanocomposites prepared by melt blending, containing 5 wt% of MA-*g*-PLA, yield a maximum in storage modulus $G'$ and a rheological plateau at low frequencies, with a content of epoxy-functionalized graphene comprised between 4 and 7 wt%. This phenomenon was ascribed to a pseudo-solid behavior resulting from the high degree of epoxy-functionalized graphene exfoliation due to strong interfacial interactions with PLA and epoxy-functionalized graphene. The better mechanical and barrier performances were obtained with PLA/GFe containing 10 wt% of epoxy-functionalized graphene and 5 wt% of MA-*g*-PLA compatibilizer. The variation of the percentage of compatibilizer showed that 5 wt% of maleated PLA was sufficient to improve the thermal, rheological, mechanical and barrier properties of the PLA nanocomposite containing 7 wt% of epoxy-functionalized graphene.

**Keywords** Nanocomposites · PLA · Maleic anhydride · Graphene · Rheology · Thermal properties mechanical properties · Water vapor permeation

✉ Kahina Issaadi
kahina.issaadi@yahoo.fr

[1] Laboratoire des Matériaux Organiques, Faculté de Technologie, Université Abderrahmane Mira, Route de Targa Ouzemour, 06000 Bejaia, Algeria

[2] Laboratoire d'Ingénierie des Matériaux de Bretagne, EA4250, Université de Bretagne Sud, Rue de Saint Maudé, 56100 Lorient, France

## Introduction

The rising oil prices helped to stimulate early interest in biodegradables back in the 1970 and concerns over the dwindling availability of landfill sites are reviving interests in biodegradable materials today [1]. Poly(lactic acid) (PLA) is emerging as the most important bio-based polyester due to its favorable properties widely investigated in various areas such as in woven and non-woven fabrics, paper coatings, food and medicine packaging, and biomedicine. The attractive price and commercial availability of lactic acid are important reasons for PLA development [2, 3].

In order to make this material more attractive for some applications, as a valid alternative to petrochemical plastics, some properties should be improved, namely mechanical resistance and gas permeability [4]. To attain these objectives, some approaches have been tried (incorporation of plasticizers, blending with other polymers, adding nanofillers) according to the required applications. Nanofillers are an interesting option, since with the addition of a small proportion, target properties can be improved, while maintaining intact other key PLA properties. Good dispersion and interfacial interaction with the polymer matrix are paramount in order for these improvements to be significant [5–10]. The nanofillers most reported are layered silicates such as montmorillonite and carbon-based nanoparticles (e.g., carbon nanotubes and graphene nanoplatelets) [11–22].

Graphene is a planar monolayer of carbon atoms arranged into a two dimensional (2D) honeycomb lattice with a carbon–carbon bond length of 0.142 nm [23]. It has attracted an enormous amount of scientific interest due to its exceptional physical properties [24]. It has been largely demonstrated that graphene incorporation can improve electrical and mechanical properties of polymers including polyethylene (PE). However, the hydrophobic nature and low polarity of PE have made effective dispersion of nanofillers difficult without compatibilization [25].

Recently, several studies have been conducted on the development and characterization of polymer/graphene nanocomposites. The incorporation of graphene has resulted in the improvement of thermal, mechanical, and electrical properties of polymer matrices [2, 13–15, 25–30]. For example, Achaby et al. [24] developed polypropylene/graphene nanocomposite in the molten state. The results of X-ray diffraction (XRD) showed good dispersion of nanosheets of graphene in the polypropylene matrix. The authors reported that increasing the graphene content resulted in a significant increase in both mechanical and thermal properties with only few percent of graphene loading. Cao et al. [31], showed that the PLA/graphene nanocomposite prepared through lyophilization method enhanced the mechanical and thermal properties of the poly-lactic acid. Kuila et al. [32] showed that graphene in the poly(methyl methacrylate) (PMMA) matrix enhanced the storage modulus and glass transition temperatures of the nanocomposites. Li et al. [33] prepared PLA/graphene nanocomposite by a method of solution blending of PLA with liquid-phase exfoliated graphene using chloroform as a mutual solvent. They showed an improvement in thermal stability and an increase of 39.57 % of the tensile strength. Recently, Wang and Lin [34] prepared the conducting

nanocomposites of surfactant-intercalated graphite oxide with MA-*g*-PLA via solution blending. The detailed morphological and X-ray diffraction results revealed that the degree of dispersion of amine surfactant-intercalated graphite oxide (GOAs) was enhanced with maleated PLA. Both the thermal and electrical conductivities showed substantial improvements with increasing GOA content.

In addition to improved mechanical, electrical and thermal properties, incorporation of graphene can significantly reduce gas permeability of polymers. Various studies [2, 35–38] showed that the reduction of gas permeability is probably associated with the high aspect ratio and surface area of graphene which provide a tortuous path for the diffusing gas molecules, enhancing the gas barrier properties compared to pristine polymer. Pinto et al. [2] investigated the permeability of PLA/graphene (GNP) and PLA/GO composites towards oxygen and nitrogen. The gas permeability decreased by threefold towards oxygen and a fourfold towards nitrogen at 0.4 wt% loading of GO or GNP. Though, it could be expected that more planar configuration of GNP would be more efficient in creating a tortuous path for permeation than GO particles, this was not observed, and both fillers showed similar effects. They explained this as the absence of orientation of the GNP platelets along the film plane, which does not contribute to increase the tortuosity in the direction perpendicular to the film plane. Zhan et al. [39]. studied the WVP properties of nanocomposites of natural rubber and graphene, finding a significant decrease in the WVP of graphene/natural rubber nanocomposites with increasing graphene content. The WVP of graphene/natural rubber nanocomposites with graphene content of 1.78 and 5.2 vol% was decreased by 40 and 60 %, respectively. Ma et al. [40] investigated the effect of graphene oxide (GO) and reduced graphene oxide (RGO) on the WVP of plasticized starch films. In the plasticized starch films containing 4 wt% of GO and 8 wt% of RGO, these authors observed a decrease of about 43 and 34 % of WVP, respectively, compared to pure starch films.

The aim of this work is to study the effect of epoxy-functionalized graphene (GFe) composition on the rheological, mechanical and barrier properties of PLA matrix containing 5 wt% of MA-*g*-PLA compatibilizer on one hand, and the effect of percentage of MA-*g*-PLA compatibilizer containing 0.44 wt% of the maleic anhydride on the dispersion of the GFe and the properties of PLA/GFe nanocomposite with 7 wt% of GFe on the other hand.

## Experimental

### Materials

PLA 7001D was supplied by Nature Works LLC. The material has a density of 1.24 g/cm$^3$, a glass transition temperature about 60 °C, and a melting point about 154 °C. The molecular weight of the material is 113,000 g/mol. MA-*g*-PLA containing 0.44 wt% of maleic anhydride is used as a compatibilizer and was synthesized as described by Issaadi et al. [41]. Epoxy-functionalized graphene (GFe) was provided by Nanovia (France). The material is composed of 90 % of carbon and 10 % of oxygen, and has a surface area of 750 m$^2$/g.

## Preparation of the samples

### Preparation of PLA/MA-*g*-PLA/xGFe nanocomposites

The preparation of nanocomposites films PLA/xGFe at different epoxy-functionalized graphene (GFe) contents, with or without MA-*g*-PLA compatibilizer was performed using melt mixing in a mini-extruder (ThermoHaake MiniLab), at 190 °C, with a screw speed of 100 rpm and a residence time of 8 min. The GFe content is between 1 and 10 wt% and that of the MA-*g*-PLA is 0, 5 and 10 wt%.

### Characterization

*Rheological experiments*

The storage modulus ($G'$) and complex viscosity ($\eta^*$) were measured as a function of angular frequency ($\omega$) using an Anton Paar, CTD 450, Physica MCR 301 rheometer. Before experiments, the samples were dried at 60 °C for 12 h and compression molded to the thickness about 2 mm. The limit of the linear viscoelastic regime was determined by performing a strain sweep at 1 Hz. The rheometer was operated in the dynamic oscillatory mode with parallel plate geometry of 25 mm diameter at 175 °C. A strain of 1 %, corresponding to the linear viscoelastic domain, was chosen to perform dynamic measurements over a frequency range of 0.001–100 Hz.

*Tensile tests*

The static tensile tests were carried out at 23 °C and at a relative humidity of 48 % according to ISO 527, using a testing apparatus (MTS Synergie RT1000). The loading speed was 1 mm $min^{-1}$. An extensometer was used with a nominal gauge length of 25 mm. The dumbbell-shaped samples with a dimension of 4 × 1.5 $mm^2$ were stamped from the compression molded sheets, using a hydraulic press equipped with two heated plates at 180 °C with a pressure of 30 bars for 3 min.

*Water vapor permeability test*

The water vapor permeations were realized using the "cups methods", referring to the standard ISO 7783. The experimental setting consists of a cylindrical vessel filled with a desiccant powder and sealed with the investigated film. 10 g of calcium chloride ($CaCl_2$) was used as the desiccant powder while temperature was set to 23 ± 1 °C with a relative humidity of 48 ± 2 %. The water mass uptake of the desiccant powder was monitored with time. The water vapor transmission rate (WVTR) was calculated from the slope of the mass uptake profile versus time as soon as the steady state was reached, using Eq. (1):

$$\mathrm{WVP} = \frac{\Delta m \times e}{A \times \Delta t \times \Delta P}, \quad (1)$$

where WVP is the water vapor permeability coefficient, $m$ is the gain of mass, $e$ is the film thickness, $A$ is the film surface, $t$ is the time and $\Delta P$ is the water vapor partial pressure difference. From the experimental conditions, the water vapor $\Delta P$ is 1400.3 Pa calculated for a temperature of 23 °C and a relative humidity of 48 %. Four films of each sample were tested.

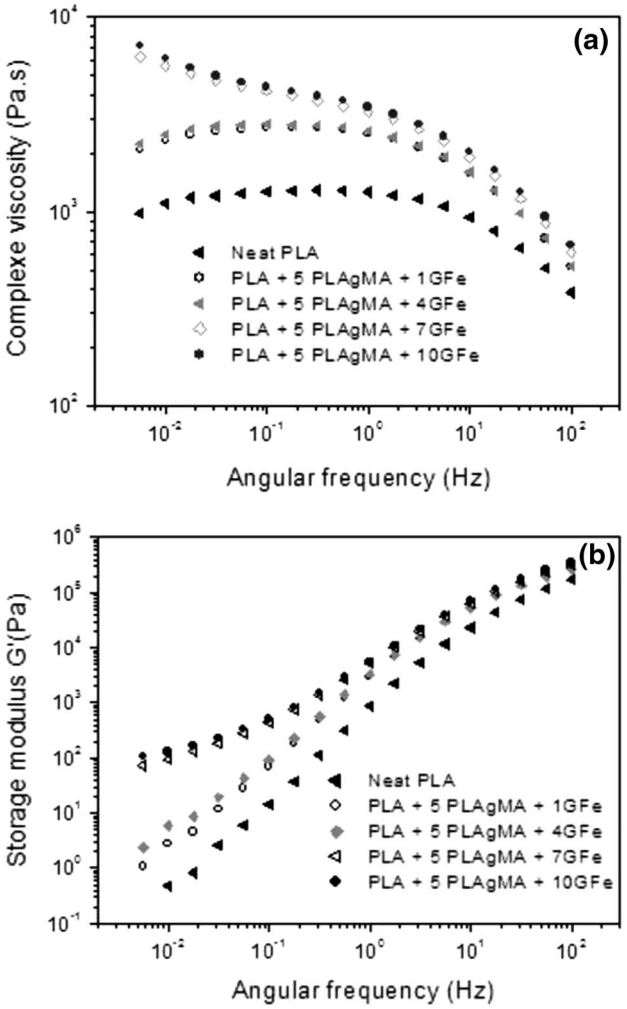


**Fig. 1** **a** Complex viscosity $\eta^*$ as a function of angular frequency of PLA/5PLAgMA/xGFe nanobiocomposites. **b** Storage modulus $G'$ as a function of angular frequency of PLA/5PLAgMA/xGFe nanobiocomposites

*Thermo-gravimetric analysis (TGA)*

Thermo-gravimetric analysis were carried out in a METTLER STAR$^e$ SW 11.00 thermal analyzer using a scanning rate of 10 °C/min under nitrogen in the temperature range starting from 20 to 800 °C, with a sample weight of about 10 mg.

## Results and discussion

### PLA/5PLAgMA/xGFe

*Rheological properties*

The effect of percentages of epoxy-functionalized graphene on the rheological, mechanical and barrier properties of PLA/5MA-*g*-PLA has been studied. A classical content of 5 wt% of MA-*g*-PLA has been chosen [41, 42] and several compositions of GFe have been used.

Neat PLA and filled PLA/5MA-*g*-PLA with various concentrations of GFe were submitted to small amplitude oscillatory shear flow at 175 °C in the frequency range $10^2$–$10^{-2}$ Hz. The rheological properties have widely been used to determine the degree of dispersion and exfoliation of nanofillers in nanocomposites [41, 43]. Figure 1a shows dependencies of the complex viscosity as a function of frequency of neat PLA and PLA/5MA-*g*-PLA nanocomposites containing 1, 4, 7 and 10 wt% of GFe.

Neat PLA exhibited a plateau in complex viscosity. For nanocomposites containing 5 wt% of MA-*g*-PLA, the complex shear viscosity clearly increased with GFe content explained by the formation of GFe networks in the PLA matrix and the transition from liquid-like to solid-like viscoelastic response. The rheological percolation threshold of PLA/5MA-*g*-PLA/xGFe nanocomposites comprised between 4 and 10 wt%. Similar phenomena have been already reported in the literature for polymers reinforced with graphene [10, 44].

The storage modulus from small strain oscillatory shear versus frequency for a series of concentrations of EFG in PLA/5MA-*g*-PLA at 175 °C are presented in the Fig. 1b. Neat PLA sample showed typical terminal behavior at low frequencies with the scaling properties of $G' \propto \omega^2$, which is in consistence with the linear viscoelastic theory [16]. However, this terminal behavior disappeared gradually with the increase of GFe loadings. The same result was observed by Li et al. [45] in poly(propylene) containing graphene nanoplatelets. As the GFe loadings reached up to 7 wt%, the PLA/5MA-*g*-PLA xGFe nanocomposites exhibited an evident solid-like response in the low-frequency region, indicating the occurrence of an elastic deformation-dominated flow. At this loading level, the particle–particle interactions among the GFe were strong enough and as a result led to the formation of percolated graphene network structures. Consequently, large-scale polymer relaxations in composites were effectively restrained by the reinforcement effect of GFe. Issaadi et al. [41], Li et al. [46] and Sabzi et al. [47] reported similar results in PLA containing silica platelets and graphene nanoplatelets.

*Mechanical properties*

Dispersion, exfoliation and homogenous distribution of GFe along with the favorable interfacial interactions between GFe and the polymer matrix are the key points needed to achieve polymer nanocomposites with enhanced final properties [13, 30, 48]. Table 1 represents the mechanical properties of the neat PLA and PLA/5MA-*g*-PLA xGFe nanocomposites with different content of graphene. The incorporation of graphene nanosheets in PLA resulted in a significant enhancement of the tensile strength and Young's modulus. Simultaneously, the elongation at break of the nanocomposites reduced with increasing graphene loading level. Incorporating 1 wt% of graphene, the Young's modulus was increased up to 3769 MPa (by 25 %). The Young's modulus of PLA/5MA-*g*-PLA containing 1 and 4 wt% EFG are close and an increase was observed for 7 and 10 wt% of GFe.

The exfoliated graphene sheets could be well dispersed in the polymer matrix, leading to a significant improvement in the mechanical properties [12, 30, 49].

*Barrier properties*

Permeability of the PLA/5MA-*g*-PLA/xGFe nanocomposite films towards the water vapor was measured using the cup method. In Table 2 are presented the water vapor permeation (WVP) of nanocomposites compared to neat PLA. Two-step decrease of WVP are observed for 1–4 and 7–10 % as the same manner that for rheological and mechanical properties. WVP of PLA/5MA-*g*-PLA/xGFe nanocomposites decrease with increasing filler content [40]. Water vapor easily permeates the PLA film and has the highest WVP value of $3.04 \times 10^{-11}$ g $m^{-1}$ $s^{-1}$ $Pa^{-1}$. Increasing the GFe content from 1 to 10 wt% leads to an obvious decrease in the WVP values of PLA/5MA-*g*-PLA + 10GFe nanocomposites (to $2.23 \times 10^{-11}$ g $m^{-1}$ $s^{-1}$ $Pa^{-1}$). GFe sheets probably introduced tortuous paths for water molecules to pass through [50]. We also observe the decrease in water vapor permeation with PLA and two different montmorillonites, Cloisite® 20A and Cloisite® 30B [41]. In the same manner as the graphene, the strong decrease in WVP is obtained with PLA containing 3 wt% of Cloisite® 20A and 5 wt% of MA-*g*-PLA.

The decrease in WVP of graphene-PLA nanocomposites suggests a great potential to use them in packaging application such as cosmetics packaging.

**Table 1** Mechanical properties of neat PLA and PLA/5PLAgMA/xGFe nanobiocomposites

| | Young's modulus (MPa) | Tensile strength (MPa) | Elongation at break (%) |
|---|---|---|---|
| Neat PLA | 3004 ± 256 | 52.7 ± 3.6 | 2.9 ± 0.1 |
| PLA + 5PLAgMA + 1GFe | 3769 ± 269 | 56.6 ± 3.4 | 2.7 ± 0.6 |
| PLA + 5PLAgMA + 4GFe | 3825 ± 214 | 54.1 ± 2.0 | 2.5 ± 0.5 |
| PLA + 5PLAgMA + 7GFe | 4471 ± 131 | 53.6 ± 2.1 | 1.6 ± 0.2 |
| PLA + 5PLAgMA + 10GFe | 4533 ± 332 | 57.1 ± 1.6 | 1.8 ± 0.5 |

**Table 2** Water vapor permeability (WVP) of neat PLA and PLA/5PLAgMA/xGFe nanobiocomposites

| | WVP · $10^{-11}$ (g/m s pa)[a] |
|---|---|
| Neat PLA | 3.04 ± 0.38 |
| PLA + 5PLAgMA +1 GFe | 2.89 ± 0.40 |
| PLA + 5PLAgMA + 4 GFe | 2.68 ± 0.11 |
| PLA + 5PLAgMA +7 GFe | 2.26 ± 0.09 |
| PLA + 5PLAgMA +10 GFe | 2.23 ± 0.07 |

[a] Calculated from the slope of the mass uptake profile versus time as soon as the steady state was reached, using Eq. (1)

## PLA/xMA-*g*-PLA/GFe nanocomposites with different percentages of MA-*g*-PLA

In this part, a content of 7 wt% of GFe was selected because of the optimum results of dispersion and percolation curve obtained in the first part of this study.

### *Rheological properties*

The viscoelastic properties of PLA/xMA-*g*-PLA nanocomposites in the presence of 7 wt% of GFe with different contents of compatibilizer are presented in Fig. 2. In Fig. 2a is presented the complex viscosity ($\eta^*$) of neat PLA and PLA/xMA-*g*-PLA nanocomposites containing 7 wt% graphene with different contents of MA-*g*-PLA. Pure PLA matrix shows a typical Newtonian behavior at low-frequency region and shear thinning behavior at high-frequency region [46]. However, compatibilized PLA/7GFe nanocomposites exhibit higher shear viscosity and earlier shear thinning behavior than pure poly(lactic acid). We notice also a significant increase of the complex viscosity slope at low frequency of the compatibilized nanocomposite.

In Fig. 2b, the pure PLA exhibits a classical curve [51]. PLA containing 7 wt% GFE shows a gradual deviation of the $G'$ slope at low frequencies indicating a "pseudo-solid-like behavior" characteristic of the formation of filler network-like structures [52]. The introduction of MA-*g*-PLA permits to obtain a higher plateau, which indicates a better exfoliation of the sheets of graphene with maleation ratio. Nevertheless, a lower storage modulus is obtained for 10 wt% maleation ratio, due to low molecular weight of MA-*g*-PLA [41].

### *Thermal stability*

Thermal stability is very important for polymeric materials as it is the limiting factor both in processing and in end-use applications [30]. The incorporation of graphene into polymer matrix permits to enhance thermal stability by acting as a superior insulator and mass transport barrier to the volatile products generated during decomposition [33].

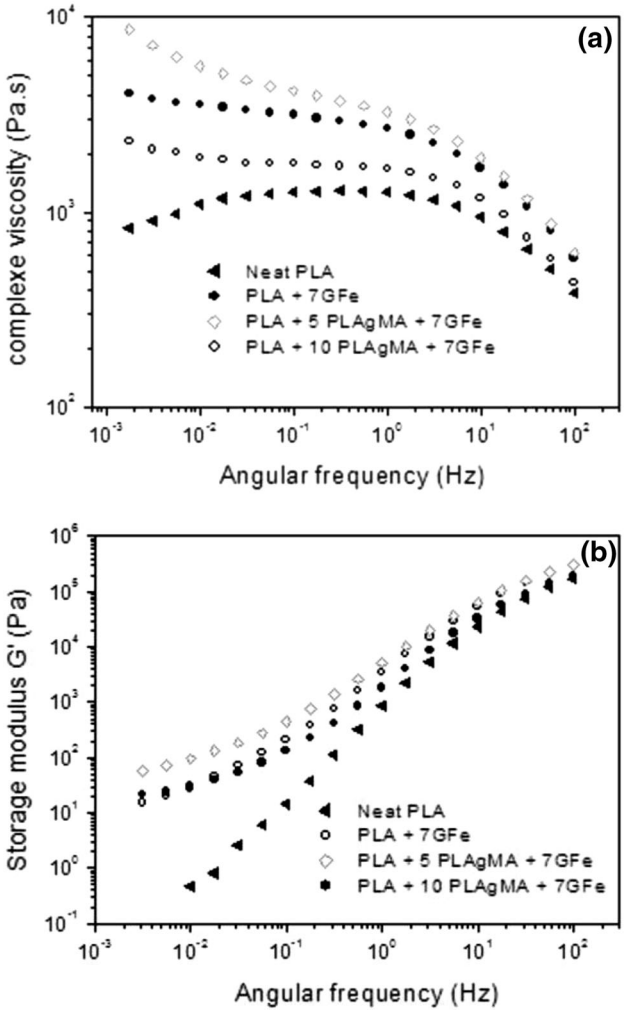


**Fig. 2** **a** Complex viscosity $\eta^*$ as a function of angular frequency of PLA/xPLAgMA/7GFe nanobiocomposites. **b** Storage modulus $G'$ as a function of angular frequency of PLA/xPLAgMA/7GFe nanobiocomposites

A content of epoxy-functionalized graphene, decomposition starting temperatures of nanobiocomposites treated with 5 and 10 wt% of MA-*g*-PLA are of the order of 327 °C. Compared to that of the non-compatibilized nanobiocomposite (315 °C) (Fig. 3), it appears that the addition of MA-*g*-PLA has a significant and drastic effect on the thermal stability of the developed nanobiocomposites. It generates a gain of 12 °C in the decomposition starting temperature. This indicates that the compatibility and interfacial adhesion nanofiller–matrix increased in the presence of the compatibilizer [10].

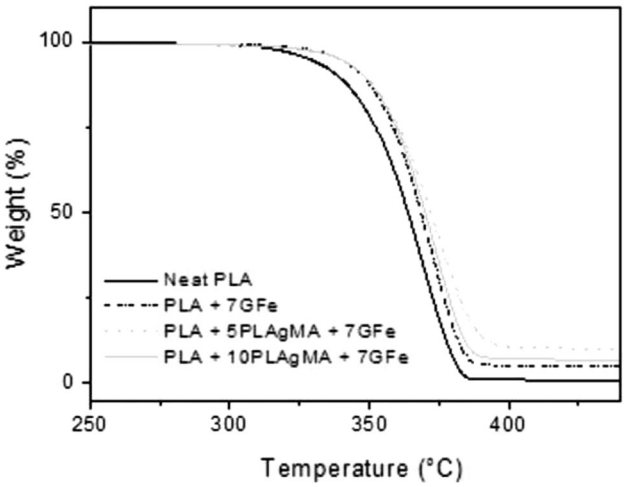


**Fig. 3** TGA thermograms of neat PLA and PLA/xPLAgMA/7GFe nanobiocomposites

*Mechanical properties*

Mechanical properties of neat PLA and PLA/xMA-*g*-PLA/GFe nanocomposites containing 7 wt% of graphene are summarized in the Table 3. The results show that the incorporation of 7 wt% of graphene functionalized epoxy with or without the presence of the compatibilizer increases the Young's modulus of the PLA matrix. This can be attributed to a significant degree of intercalation and a non-negligible degree of exfoliation, resulting in a greater mineral–PLA matrix interfacial area [53]. The presence of 5 wt% of MA-*g*-PLA results in an increase of the Young's modulus of about 49 %, as compared with neat PLA value. Coupling agents such as MA-*g*-PLA are effective compatibilizer that help improve interfacial adhesion by forming covalent and hydrogen bonds between graphene and PLA which facilitates the transfer of stress between the filler and matrix [42].

There is no significant change in the tensile strength of neat PLA and their nanocomposites. However, the elongation at break decrease with the addition of GFe and the lower value is obtained in the presence of 5 and 10 wt% of MA-*g*-PLA.

**Table 3** Mechanical properties of neat PLA and PLA/xPLAgMA/7GFe nanobiocomposites

| | Young's modulus (MPa) | Tensile strength (MPa) | Elongation at break (%) |
|---|---|---|---|
| Neat PLA | 3004 ± 256 | 52.7 ± 3.6 | 2.9 ± 0.1 |
| PLA + 7GFe | 3899 ± 237 | 51.4 ± 4.6 | 2.2 ± 0.4 |
| PLA + 5PLAgMA + 7GFe | 4471 ± 131 | 53.6 ± 2.1 | 1.6 ± 0.2 |
| PLA + 10PLAgMA + 7GFe | 4025 ± 197 | 49.1 ± 3.5 | 1.6 ± 0.2 |

The reason may be attributed to a large aspect ratio and the interaction between graphene and the matrix, which restricts the movement of the polymer chains [54].

These results are in accordance with rheological measurements and can be explained by the high compatibility between the PLA and the graphene in the presence of 5 wt% of MA-*g*-PLA.

The improvement in tensile properties at low nanofiller loading has already been reported in the literature. For example Wang et al. were recorded a 21 % increase in tensile strength with the addition of 2 wt% of graphene nanosheet (GNS) in the poly(butylene succinate) [15].

*Barrier properties*

The water vapor permeability (WVP) of PLA and graphene-based polymer was investigated using the "Cup method" at 23 °C and 50 % RH. In Table 4, a decrease in WVP of the PLA/GFe nanocomposites with or without compatibilizer, is obtained comparing to the neat PLA sample. The decrease in gas permeability is attributed to the barrier properties of the layers of nanofiller dispersed in the polymer matrix [55]. It should be noted that the nanocomposite compatibilized with 5 wt% of MA-*g*-PLA results in a considerable decrease in water vapor permeability. These observations revealed that GFe is well dispersed in the presence of 5 wt% of compatibilizer. A slight increase of WVP was then observed with the incorporation of 10 wt% of maleated PLA.

The results obtained by barrier properties are in concordance with those obtained by rheology and mechanical properties.

## Conclusion

The PLA nanocomposite samples comprising epoxy-functionalized graphene were prepared by melt mixing method. The effect of the content of graphene has been studied on the rheological, mechanical and barrier properties of the nanocomposites PLA/5MA-*g*-PLA/xGFe. In this section of our study, we noticed an improvement of the studied properties with the enhanced of the content of epoxy-functionalized graphene.

**Table 4** Vapor permeability (WVP) of neat PLA and PLA/xPLAgMA/7GFe nanobiocomposites

| | WVP · $10^{-11}$(g/m s pa)[a] |
|---|---|
| Neat PLA | 3.04 ± 0.38 |
| PLA + 7GFe | 2.52 ± 0.15 |
| PLA + 5PLAgMA + 7GFe | 2.26 ± 0.09 |
| PLA + 10PLAgMA + 7GFe | 2.65 ± 0.16 |

[a] Calculated from the slope of the mass uptake profile versus time as soon as the steady state was reached, using Eq. (1)

In order to examine the effect of the percentage of compatibilizer, a content of 7 wt% of EFG was selected, because of the optimum results of the dispersion in the PLA/5MA-*g*-PLA matrix. The results showed that the best rheological and the greatest thermal, mechanical and barrier properties were obtained for the nanocomposite containing 7 wt% of graphene and 5 wt% of compatibilizer (PLA/5MA-*g*-PLA/7GFe).

## References


1. Mohanty AK, Misra M, Hinrichsen G (2000) Biofibres, biodegradable polymers and biocomposites: an overview. Macromol Mater Eng 276:1–24
2. Pinto AM, Cabral J, David A, Tanaka DAP, Mendes AMM, Magalhaes FD (2013) Effect of incorporation of graphene oxide and graphene nanoplatelets on mechanical and gas permeability properties of poly(lactic acid) films. Polym Int 62:33–40
3. Lasprilla AJR, Martinez GAR, Lunelli BH et al (2010) Synthesis and characterization of poly (lactic acid) for use in biomedical field. Chem Eng 24:985–990
4. Cabedo L, Luis FJ, Pilar VM, Lagarón JM et al (2006) Optimization of biodegradable nanocomposites based on aPLA/PCL blends for food packaging applications. Macromol Symp 233:191–197
5. Li M-C, Cho UR (2013) Effectiveness of coupling agents in the poly (methylmethacrylate)-modified starch/styrene-butadiene rubber interfaces. Mater Lett 92:132–135
6. Li M-C, Ge X, Cho UR (2013) Emulsion grafting vinyl monomers onto starch for reinforcement of styrene-butadiene rubber. Macromol Res 21:519–528
7. Li M-C, Ge X, Cho UR (2013) Mechanical performance, water absorption behavior and biodegradability of poly (methyl methacrylate)-modified starch/SBR biocomposites. Macromol Res 21:793–800
8. Li M-C, Zhang Y, Cho UR (2014) Mechanical, thermal and friction properties of rice bran carbon/nitrile rubber composites: influence of particle size and loading. Mater Design 63:565–574
9. Ge X, Li M-C, Cho UR (2015) Novel one-step synthesis of acrylonitrile butadiene rubber/bentonite nanocomposites with (3-mercaptopropyl) trimethoxysilane as a compatibilizer. Polym Compos 36:1693–1702
10. Issaadi K, Habi A, Grohens Y, Pillin I (2016) Maleic anhydride-grafted poly(lactic acid) as a compatibilizer in poly(lactic acid)/graphene oxide nanocomposites. Polym Bull. doi:10.1007/s00289-015-1593-z
11. Kim SJ, Shin BS, Hong JL et al (2001) Reactive compatibilization of the PBT/EVA blend by maleic anhydride. Polymer 42:4073–4080
12. Zhou K, Gu SY, Zhang YH et al (2012) Effect of dispersion on rheological and mechanical properties of polypropylene/carbon nanotubes nanocomposites. Polym Eng Sci 52:1485–1494
13. Zhang L, Li Y, Wang H et al (2014) Strong and ductile poly (lactic acid) nanocomposite films reinforced with alkylated graphene nanosheets. Chem Eng J 264:538–546
14. Yuan X (2011) Enhanced interfacial interaction for effective reinforcement of poly (vinyl alcohol) nanocomposites at low loading of graphene. Polym Bull 67:1785–1797
15. Wang X, Yang H, Song L et al (2011) Morphology, mechanical and thermal properties of graphene-reinforced poly(butylene succinate) nanocomposites. Compos Sci Technol 72:1–6
16. Wang B, Wan T, Zeng W (2011) Dynamic rheology and morphology of polylactide/organic montmorillonite nanocomposites. Appl Polym Sci 121:1032–1039
17. Kim H, Macosko CW (2009) Processing–property relationships of polycarbonate/graphene composites. Polymer 50:3797–3809
18. Song P, Cao Z, Cai Y et al (2011) Fabrication of exfoliated graphene-based polypropylene nanocomposites with enhanced mechanical and thermal properties. Polymer 52:4001–4010
19. Zanetti M, Lomakin S, Camino G (2000) Polymer layered silicate nanocomposites. Macromol Mater Eng 279:1–9
20. Renard E, Walls M, Guérin P, Langlois V (2004) Hydrolytic degradation of blends of polyhydroxyalkanoates and functionalized polyhydroxyalkanoates. Polym Degrad Stab 85:779–787

21. McNally T, Pötschke P, Halley P et al (2005) Polyethylene multiwalled carbon nanotube composites. Polymer 46:8222–8232
22. Lee JI, Yang SB, Jung HT (2009) Carbon nanotubes–polypropylene nanocomposites for electrostatic discharge applications. Macromolecules 42:8328–8334
23. Galpaya D, Wang M, Liu M, Motta N, Waclawik E, Yan C (2012) Recent advances in fabrication and characterization of graphene–polymer nanocomposites. Graphene 1:30–49
24. Geim AK, Novoselov KS (2007) The rise of graphene. Nat Mater 6:183–191
25. Kim H, Kobayashi S, AbdurRahim MA (2011) Graphene/polyethylene nanocomposites: effect of polyethylene functionalization and blending methods. Polymer 52:1837–1846
26. Kuila T, Bose S, Khanra P et al (2011) Characterization and properties of in situ emulsion polymerized poly (methyl methacrylate)/graphene nanocomposites. Compos Part A Appl Sci Manuf 42:1856–1861
27. Zaman I, Phan TT, Kuan HC (2011) Epoxy/graphene platelets nanocomposites with two levels of interface strength. Polymer 52:1603–1611
28. Sridhar V, Lee I, Chun HH, Park H (2013) Graphene reinforced biodegradable poly(3-hydroxybutyrate-co-4-hydroxybutyrate) nano-composites. Express Polym Lett 7:20–328
29. Domingues SH, Salvatierra RV, Oliveira MM (2011) Transparent and conductive thin films of graphene/polyaniline nanocomposites prepared through interfacial polymerization. Chem Commun 47:2592–2594
30. El Achaby M, Arrakhiz FE, Vaudreuil S et al (2012) Mechanical, thermal, and rheological properties of graphene-based polypropylene nanocomposites prepared by melt mixing. Polym Compos 33:733–744
31. Cao Y, Feng J, Wu P (2010) Preparation of organically dispersible graphene nanosheet powders through a lyophilization method and their poly(lactic acid) composites. Carbon 48:3834–3839
32. Kuila T, Bose S, Khanra P, Kim NH, Rhee KY, Lee JH (2011) Characterization and properties of in situ emulsion polymerized poly (methyl methacrylate)/graphene nanocomposites. Compos Part A Appl Sci Manuf 42:1856–1861
33. Li X, Xiao Y, Bergeret A, Longerey M, Che J (2014) Preparation of polylactide/graphene composites from liquid phase exfoliated graphite sheets. Polym Compos 35:396–403
34. Li X, Xiao Y, Bergeret A, Longerey M, Che J (2014) Preparation and characterization of maleated polylactide-functionalized graphite oxide nanocomposites. Polym Res 334:3–14
35. Huang HD, Ren PG, Chen J, Zhang WQ, Ji X, Li ZM (2012) High barrier graphene oxide nanosheet/poly (vinyl alcohol) nanocomposite films. Membr Sci 410:156–163
36. Kim HM, Lee HS (2014) Water and oxygen permeation through transparent ethylene vinyl alcohol/(graphene oxide) membranes. Carbon Lett 15:50–56
37. Chang CH, Huang TC, Peng CW (2012) Novel anticorrosion coatings prepared from polyaniline/graphene composites. Carbon 50:5044–5051
38. Compton OC, Kim S, Pierre C, Torkelson JM, Nguyen ST (2010) graphene nanosheets as highly effective barrier property enhancers. Adv Mater 22:4759–4763
39. Zhan Y, Lavorgna M, Buonocore G, Xia H (2012) Enhancing electrical conductivity of rubber composites by constructing interconnected network of self-assembled graphene with latex mixing. Mater Chem 22:10464–10468
40. Ma T, Chang PR, Zheng P, Ma X (2013) The composites based on plasticized starch and graphene oxide/reduced graphene oxide. Carbohydr Polym 94:63–70
41. Issaadi K, Habi A, Grohens Y, Pillin I (2015) Effect of the montmorillonite intercalant and anhydride maleic grafting on polylactic acid structure and properties. Appl Clay Sci 107:62–69
42. Nyambo C, Mohanty AK, Misra M (2011) Effect of maleated compatibilizer on performance of PLA/wheat straw-based green composites. Macromol Mater Eng 296:710–718
43. Cassagnau P (2008) Melt rheology of organoclay and fumed silica nanocomposites. Polymer 49:2183–2196
44. Kim H, Abdala AA, Macosko CW (2010) Graphene/polymer nanocomposites. Macromolecules 43:6515–6530
45. Li Y, Zhu J, Wei S, Ryu J, Sun L, Guo Z (2011) Poly (propylene)/graphene nanoplatelet nanocomposites: melt rheological behavior and thermal, electrical, and electronic properties. Macromol Chem Phys 112:1951–1959
46. Li Y, Han C, Bian J, Han L, Dong L, Gao G (2012) Rheology and biodegradation of polylactide/silica nanocomposites. Polym Compos 33:1719–1727

47. Sabzi M, Jiang L, Liu F, Ghasemi I, Atai M (2013) Graphene nanoplatelets as polylactic acid modifier: linear rheological behavior and electrical conductivity. Mater Chem A 1:8253–8261
48. Liang J, Huang Y, Zhang L, Wang Y, Ma Y, Guo T, Chen Y (2009) Molecular-level dispersion of graphene into poly (vinyl alcohol) and effective reinforcement of their nanocomposites. Adv Funct Mater 19:2297–2302
49. Jiang L, Shen X-P, Wu J-L, Shen K-C (2010) Preparation and characterization of graphene/poly (vinyl alcohol) nanocomposites. Appl Polym Sci 118:275–279
50. Liu D, Chang PR, Deng S (2011) Fabrication and characterization of zirconium hydroxide-carboxymethyl cellulose sodium/plasticized *Trichosanthes kirilowii* starch nanocomposites. Carbohydr Polym 86:1699–1704
51. Darie RN, Pâslaru E, Sdrobis A et al (2014) Effect of nanoclay hydrophilicity on the poly (lactic acid)/clay nanocomposites properties. Ind Eng Chem Res 53:7877–7890
52. Filippone G, deLuna MS, Acierno D, Russo P (2012) Elasticity and structure of weak graphite nanoplatelet (GNP) networks in polymer matrices through viscoelastic analyses. Polymer 53:2699–2704
53. Zaidi L, Bruzaud S, Bourmaud A (2010) Relationship between structure and rheological, mechanical and thermal properties of polylactide/cloisite 30B nanocomposites. Appl Polym Sci 116:1357–1365
54. Zhao X, Zhang Q, Chen D, Lu P (2010) Enhanced mechanical properties of graphene-based poly(vinyl alcohol) composites. Macromolecules 43:2357–2363
55. Żenkiewicz M, Richert J (2008) Permeability of polylactide nanocomposite films for water vapour, oxygen and carbon dioxide. Polym Test 27:835–840